RESEARCH ARTICLE

WILEY

Characterization of human skin equivalents developed at body's core and surface temperatures

Arnout Mieremet[1] (iD) | **Rianne van Dijk[2]** | **Walter Boiten[2]** | **Gert Gooris[2]** |
Joke A. Bouwstra[2] | **Abdoelwaheb El Ghalbzouri[1]**

[1] Department of Dermatology, Leiden University Medical Centre, Leiden, The Netherlands

[2] Research division BioTherapeutics, LACDR, Leiden University, Leiden, The Netherlands

Correspondence
Arnout Mieremet, Department of Dermatology, Leiden University Medical Centre, Leiden 2333ZA, The Netherlands.
Email: a.mieremet@lumc.nl

Abstract

Human skin equivalents (HSEs) are in vitro developed three-dimensional models resembling native human skin (NHS) to a high extent. However, the epidermal lipid biosynthesis, barrier lipid composition, and organization are altered, leading to an elevated diffusion rate of therapeutic molecules. The altered lipid barrier formation in HSEs may be induced by standardized culture conditions, including a culture temperature of 37°C, which is dissimilar to skin surface temperature. Therefore, we aim to determine the influence of culture temperature during the generation of full thickness models (FTMs) on epidermal morphogenesis and lipid barrier formation. For this purpose, FTMs were developed at conventional core temperature (37°C) or lower temperatures (35°C and 33°C) and evaluated over a time period of 4 weeks. The stratum corneum (SC) lipid composition was analysed using advanced liquid chromatography coupled to mass spectrometry analysis. Our results show that SC layers accumulated at a similar rate irrespective of culture temperature. At reduced culture temperature, an increased epidermal thickness, a disorganization of the lower epidermal cell layers, a delayed early differentiation, and an enlargement of granular cells were detected. Interestingly, melanogenesis was reduced at lower temperature. The ceramide subclass profile, chain length distribution, and level of unsaturated ceramides were similar in FTMs generated at 37°C and 35°C but changed when generated at 33°C, reducing the resemblance to NHS. Herein, we report that culture temperature affects epidermal morphogenesis substantially and to a lesser extent the lipid barrier formation, highlighting the importance of optimized external parameters during reconstruction of skin.

KEYWORDS

artificial skin, cell culture techniques, ceramides, lipids, morphogenesis, skin temperature, tissue engineering

1 | INTRODUCTION

Tissue engineered human skin equivalents (HSEs) mimic many properties of native human skin (NHS). However, several aspects of in vitro tissue reconstruction need to be studied and optimized to further increase the resemblance to NHS, to understand the underlying biology, and to improve in vitro–in vivo correlations (Boyce, 1996; Gordon et al., 2015; Niehues et al., 2018; Planz, Lehr, & Windbergs, 2016). The main barrier of the skin resides in the uppermost layer of the epidermis, which is termed the stratum corneum (SC; Proksch, Brandner, & Jensen, 2008). This layer is made of corneocytes embedded in a lipid matrix. The composition of the lipid matrix affects the lamellar and lateral organization. The lipid organization has a profound impact on the rate of penetration of therapeutic compounds through the intercellular route when applied topically (Boncheva, 2014; Bouwstra, Honeywell-Nguyen, Gooris, & Ponec, 2003). Compared with NHS, the barrier formation of HSEs is altered, leading to an elevated in vitro diffusion rate and uncertainty in in vitro–in vivo correlations (Regnier, Caron, Reichert, & Schaefer, 1993; Schmook, Meingassner, & Billich, 2001; Schreiber et al., 2005; Thakoersing et al., 2011).

The most abundant lipid classes within the SC matrix are cholesterol, free fatty acids, and ceramides. The latter can vary in headgroup architecture and carbon chain length and are crucial for the formation of lipid lamellae in the SC lipid matrix (Eichner et al., 2016; Mojumdar et al., 2016). In this study, we specified these as total ceramides (CERs$_{total}$), which covers both the acylceramide subclasses (CERs EO) and the (non-ω-O) ceramide subclasses (CERs). Several studies reported the differences in lipid composition between HSEs and NHS, which encompasses an altered CERs$_{total}$ subclass profile and CERs$_{total}$ carbon chain length distribution (Thakoersing et al., 2011; Thakoersing et al., 2013). Additionally, the level of unsaturated CERs within the SC of HSEs is higher as compared with NHS. These compositional differences directly affect the organization and functionality of the lipid matrix (Mojumdar, Kariman, van Kerckhove, Gooris, & Bouwstra, 2014).

To form the lipid barrier matrix, many precursor lipid entities are synthesized by keratinocytes (Feingold & Elias, 2014). To attain the proper amounts and classes of barrier lipids, the proliferation/differentiation processes of keratinocytes need to be in homeostasis. Many factors can influence the proliferation/differentiation balance in vitro, including level of nutrients and/or waste products in the culture medium and external environmental factors (Ponec et al., 1997; Ponec, Weerheim, Kempenaar, Mommaas, & Nugteren, 1988; Stark, Baur, Breitkreutz, Mirancea, & Fusenig, 1999). The first studies on modulating environmental factors in vitro were reported in 1997 (Gibbs et al., 1997; Ponec et al., 1997). Key hypothesis in these studies was that the proliferation/differentiation balance of in vitro HSE cultures is altered due to the difference in temperature between in vivo (28–32°C; Pinnagoda, Tupkek, Agner, & Serup, 1990) and in vitro (37°C). In fact, these studies have reported that incubation of primary keratinocytes at reduced temperature (from 37°C to 33°C) affected epidermal morphogenesis directly. Recently, this has been confirmed by using monocultures and an ex vivo skin barrier repair model (Bidaux et al., 2015;

Bidaux, Borowiec, Prevarskaya, & Gordienko, 2016; Borowiec, Delcourt, Dewailly, & Bidaux, 2013; Danso, Berkers, Mieremet, Hausil, & Bouwstra, 2015; Viano, Alotto, Aillon, Castagnoli, & Silvagno, 2017). However, there is still considerable uncertainty to what extent the culture temperature affects the development of three-dimensional (3D) HSEs and whether or to what extent this affects the CERs$_{total}$ composition.

In this study, we aim to determine the influence of culture temperature on epidermal morphogenesis and lipid barrier formation. For this purpose, full thickness models (FTMs) were developed at conventional body's core temperature (37°C) and at reduced temperatures (35°C and 33°C), better approaching that of skin surface temperature.

2 | MATERIALS AND METHODS

2.1 | Primary cell isolation

Primary human fibroblasts and keratinocytes were isolated from female adult surplus human breast skin, aged between 23 to 63 years old and Fitzpatrick skin photo-type classification I to III. Obtainment of healthy tissue was performed following the Declaration of Helsinki principles, as described before (Haisma et al., 2013). The dermis and epidermis were split after overnight incubation in 2.4-U/ml dispase II (Roche, Almere, The Netherlands). The epidermis was incubated in 0.05% (w/v) trypsin (BD Falcon, Breda, The Netherlands), and primary keratinocytes were isolated and cultured in Dulbecco's Modified Eagle's Medium diluted 3:1 in Ham's F12 (Gibco, Paisley, Scotland) supplemented with 5% foetal bovine serum (Hyclone, Logan, UT, USA), 100-µg/ml penicillin/streptomycin, 1-µM hydrocortisone, 1-µM isoproterenol, and 0.087-µM insulin (Sigma, Zwijndrecht, The Netherlands; El Ghalbzouri, Commandeur, Rietveld, Mulder, & Willemze, 2009). The dermis was incubated in a 3:1 (w/w) mixture of collagenase (ThermoFischer, Bleiswijk, The Netherlands) and dispase II for two 2 hours at 37°C, and primary fibroblasts were isolated and cultured in Dulbecco's Modified Eagle's Medium supplemented with 5% foetal bovine serum, and 100-µg/ml penicillin/streptomycin (El Ghalbzouri et al., 2009; van Drongelen et al., 2014). All primary cell cultures were tested negative for mycoplasma contamination.

2.2 | Generation of FTMs

FTMs were produced using a transwell system on filter inserts (Corning Transwell cell culture inserts, membrane diameter 24 mm, pore size 3 µm; Corning Life Sciences, The Netherlands). To form the 3D dermal equivalent, a suspension of rat tail tendon collagen (4 mg/ml) was mixed with Hank's Balanced Salt Solution, 0.1% acetic acid, pH corrected to neutral with NaOH, and enriched with 10% foetal bovine serum. With this suspension, a 1-ml cell free bottom layer and a 3-ml fibroblast containing top layer (1.2×10^5 cells/dermal equivalent) were formed. After 1 week, primary keratinocytes (2.5×10^5/model) in their first passage were seeded onto each dermal

equivalent and cultured as described extensively before (Thakoersing et al., 2011). Reduction in temperature occurred at once on Day 4 after air exposure using the Memmert INC153med CO_2 incubator (Memmert, Schwabach, Germany). At least three biological replicates of FTMs were generated and were harvested 7, 14, 21, and 28 days after air exposure.

2.3 | Morphology and protein expression

2.3.1 | Fixation of the tissue

FTMs were snap frozen in liquid nitrogen using gelatin capsules filled with Tissue-Tek® O.C.T.™ Compound (Sakura Finetek Europe B.V., Alphen aan den Rijn, The Netherlands) or fixated with 4% formaldehyde (Added Pharma, Oss, The Netherlands), dehydrated and paraffin embedded (Mieremet et al., 2017).

2.3.2 | Immunohistochemical analyses

Immunohistochemical analyses were performed on 5-μm sliced formalin-fixed paraffin embedded (FFPE) tissue sections. These were stained with haematoxylin and eosin (Klinipath, Duiven, The Netherlands) according to manufacturer's instructions. For protein expression by immunohistochemistry, tissue sections were deparaffinized and rehydrated to perform heat-mediated antigen retrieval in citrate buffer (pH 6). Thereafter, sections were blocked with 2% normal human serum (Sanquin, Leiden, The Netherlands) followed by application of the primary and sequentially the secondary antibody, as described earlier (Mieremet, Rietveld, van Dijk, Bouwstra, & El Ghalbzouri, 2018). Details of utilized primary and secondary antibody are described in Table S1. No primary antibody was applied on sections for negative control. Images were postprocessed by cropping and equally colour matched using Adobe Photoshop (CS6 version 13.0) to reduce interbatch variability. No immunoreactivity of the secondary antibodies was detected in all stainings (Figure S1a).

2.3.3 | Immunofluorescence analyses

For protein expression by immunofluorescence, 5-μm FFPE sections were deparaffinized and rehydrated to perform heat-mediated antigen retrieval in citrate buffer (pH 6) as described earlier (Mieremet, et al., 2018). Antigen retrieval for collagen type IV staining occurred using FFPE sections treated for 40 min with a 0.025% protease solution (Sigma). Laminin 332 staining was performed on 5-μm frozen sections, dried overnight, and fixed in acetone for 10 min. Visualization of the sections occurred using a fluorescence microscope (Leica CTR5000, Leica, Wetzlar, Germany). Images were equally postprocessed by cropping using Adobe Photoshop for better presentation.

2.3.4 | Determination of the number of corneocytes layers

Frozen sections were sliced 5 μm using a cryotome (Leica CM3050S), dried overnight, and fixed in acetone for 10 min. Sections were stained for 1 min with a 1% (w/v) safranin O (Sigma) solution dissolved in Millipore water. After Millipore water washout, a 2% (w/v) potassium hydroxide (KOH) solution was applied for 10–15 min to swell the corneocytes. Slides were sealed with a cover glass and imaged immediately. Per sample, four technical replicates were examined.

2.3.5 | Estimation of epidermal thickness and proliferation index

The epidermal thickness was determined through quantification of six to eight images per sample of various regions. The outline of the viable epidermis area was measured with Adobe Photoshop (CS6 version 13.0) in pixels and transformed to squared micrometres. The proliferation index was determined through counting the number of Ki67 positive nuclei in the basal and suprabasal layer in a region of 100 basal cells. The resulting proliferation index is the percentage of Ki67 positive nuclei in at least three different regions per sample.

2.3.6 | Melanin content

Fontana-Masson silver staining was performed on 5-μm FFPE sections after deparaffinization and rehydratation. Ammoniacal silver solution was prepared by adding ammonia solution to 5% (w/v) silver nitrate (Sigma) until the solution was clear. Slides were incubated for 20 min with this ammoniacal silver solution at 60°C followed by Millipore water washout and 90 s incubation in 0.1% gold chloride solution (Sigma). Afterwards, incubation for 2 min in 2% (w/v) sodium thiosulfate and counterstaining with nuclear fast red (Sigma) was performed. Images were obtained using the light microscope. At least three technical replicates for a minimum of two biological replicates were analysed with Image J Software (NIH, Bethesda, MD).

2.4 | SC isolation and small angle X-ray diffraction analysis

SC was isolated from the skin, air-dried, and stored under Argon gas over silica until further use as described before (Bouwstra, Gooris, van der Spek, & Bras, 1991; Mieremet, et al., 2017). Small-angle X-ray diffraction measurements were performed at the European Synchrotron Radiation Facility (Grenoble, France) at station BM26B for a period of 2 × 150 s as described elsewhere (Mieremet, et al., 2017; Mojumdar, Kariman, et al., 2014). From the positions of a series of equidistant diffraction peaks (located at q_n), the repeat distance (d) of a lamellar phase was calculated using the equation $d = n \cdot 2\pi/q_n$, where n is the order number of the diffraction peak.

2.5 | Lipid extraction and liquid chromatography–mass spectrometry analysis

Extraction of total lipids from isolated SC of FTMs after 14 and 28 days was cultured, and NHS was performed with an adjusted Bligh and Dyer method as described by Boiten et al. (2016). To determine the weight percentage of lipids in the SC, dry SC weight was measured before and after extraction. The lipids were analysed and quantified using normal phase liquid chromatography–mass spectrometry according to the method described by Boiten et al. The sample concentration of SC extracts was set at 0.3 mg/ml, and 5 μl was injected. SC lipid extracts were separated on a PVA-Sil column (5-μm particles, 100 × 2.1-mm i.d.; YMC, Kyoto, Japan), and CERs$_{total}$ were detected with an Acquity UPLC H-class (Waters, Milford, MA, USA) coupled to an XEVO TQ-S mass spectrometer (Waters). Measurements were performed in full scan mode from 1.25–8.00 min between m/z 350 and 1,350 and from 8.0 to 12.5 min between m/z 500 and 1,350. Ceramide N(24deuterated) S(18) was used as internal standard (ISTD). Predicted response factors for quantification were calculated using the response over mass (Figure S2). For ceramides AS, NP, and NS, the signal was corrected for overlap of unsaturated ceramides containing two naturally abundant ^{13}C. Nomenclature of the CER subclasses is followed according to Motta et al. (1993).

2.6 | Statistics

Statistical analyses were conducted using GraphPad Prism version 7.00 for Windows (GraphPad Software, La Jolla, California, USA). In general, statistical testing was performed after D'Agostino and Pearson normality testing with one-way or two-way analysis of variance with Tukey's multiple comparisons posttesting, otherwise indicated. Significance is shown for comparison between FTMs (with lines and asterisk) and for comparison of FTMs to NHS (by NHS), otherwise indicated. Statistical differences are noted as *, **, or ***, corresponding to $p < .05$, $<.01$, and <0.001.

3 | RESULTS

3.1 | Epidermal development at various temperatures over time

The developed FTMs were cultured at different temperatures (37°C, 35°C, and 33°C) and examined 7, 14, 21, and 28 days after air exposure macroscopically (Figure 1a). We observed increased skin colouring in FTMs cultured at 37°C, strongest after 21–28 days. Surprisingly, this colouring was reduced or absent in FTMs generated at lower temperature. Assessment of general morphology revealed that the basal and lower spinous layers were less organized at reduced culture temperature, as the transition between columnar shaped keratinocytes in the basal layer and polygonal to flattened shaped keratinocytes in the spinous layer was less clear (Figure 1b). At 37°C,

the granular cells flatten over time, resulting in a higher resemblance to the morphology of granular cells in NHS between 21 and 28 days after air exposure. This is less evident in FTMs developed at reduced temperatures, in which the granular cells remained enlarged. The thickness of the viable epidermis was increased at lower culture temperature, most pronounced at 33°C (Figure 1c). Although the epidermal thickness decreased over time, eventually to levels comparable with NHS, at reduced temperature the viable epidermis remained thicker during the entire culture period. The SC thickness was determined by quantification of the number of corneocyte layers after safranin red staining (Figure S1b). The number of corneocyte layers increased over time and mimics that of NHS between 12 and 20 days after air exposure (Figure 1d). Between the different temperatures, no significant differences were observed in the linear rate of accumulation in corneocyte layers. Extrapolation of the data revealed that the first SC layers were formed on 4–5 days after air exposure, which is also the time point of temperature reduction during development of FTMs.

3.2 | Morphogenesis at various temperatures over time

To gain more insights into the proliferation/differentiation balance of FTMs generated at reduced temperatures, the epidermal morphogenesis was evaluated from apical to basal side by immunohistochemical analyses (Figure 2a). The late and terminal differentiation programs were assessed by loricrin, involucrin, and filaggrin expression. Both loricrin and filaggrin were located at the stratum granulosum similarly in FTMs and in NHS. Involucrin was expressed at lower layers in the epidermis of FTMs, contrary to NHS. These examinations confirmed the enlargement of granular cells in FTMs generated at reduced temperature. Epidermal cell activation was determined by the expression of keratin 16. This protein remained expressed in all conditions over time, in contrast to its absence in NHS. At reduced temperature, the expression of the early differentiation marker keratin 10 is delayed. The proliferation index was determined for both the basal and suprabasal Ki67 positive cells (Figure 2b). At reduced temperature, the basal layer proliferation index was lower, whereas it was higher for suprabasal positive cells. Finally, we assessed the deposition of basement membrane proteins. Over time, an increased expression of collagen type IV and laminin 332 was observed. When comparing the FTMs developed at different temperatures, the deposition of collagen type IV is continuous but delayed at 35°C and 33°C.

3.3 | Melanogenesis in the viable epidermis

Further investigation on the skin colouring in FTMs generated at 37°C, 35°C, and 33°C was performed by visualizing the melanin content (Figure 3a). The melanin in the FTMs was less abundant at reduced temperature and more abundant at later time points, in line with the macroscopic observations (Figure 1a). Quantification of the melanin content in the viable epidermis revealed a significant reduction of melanin in
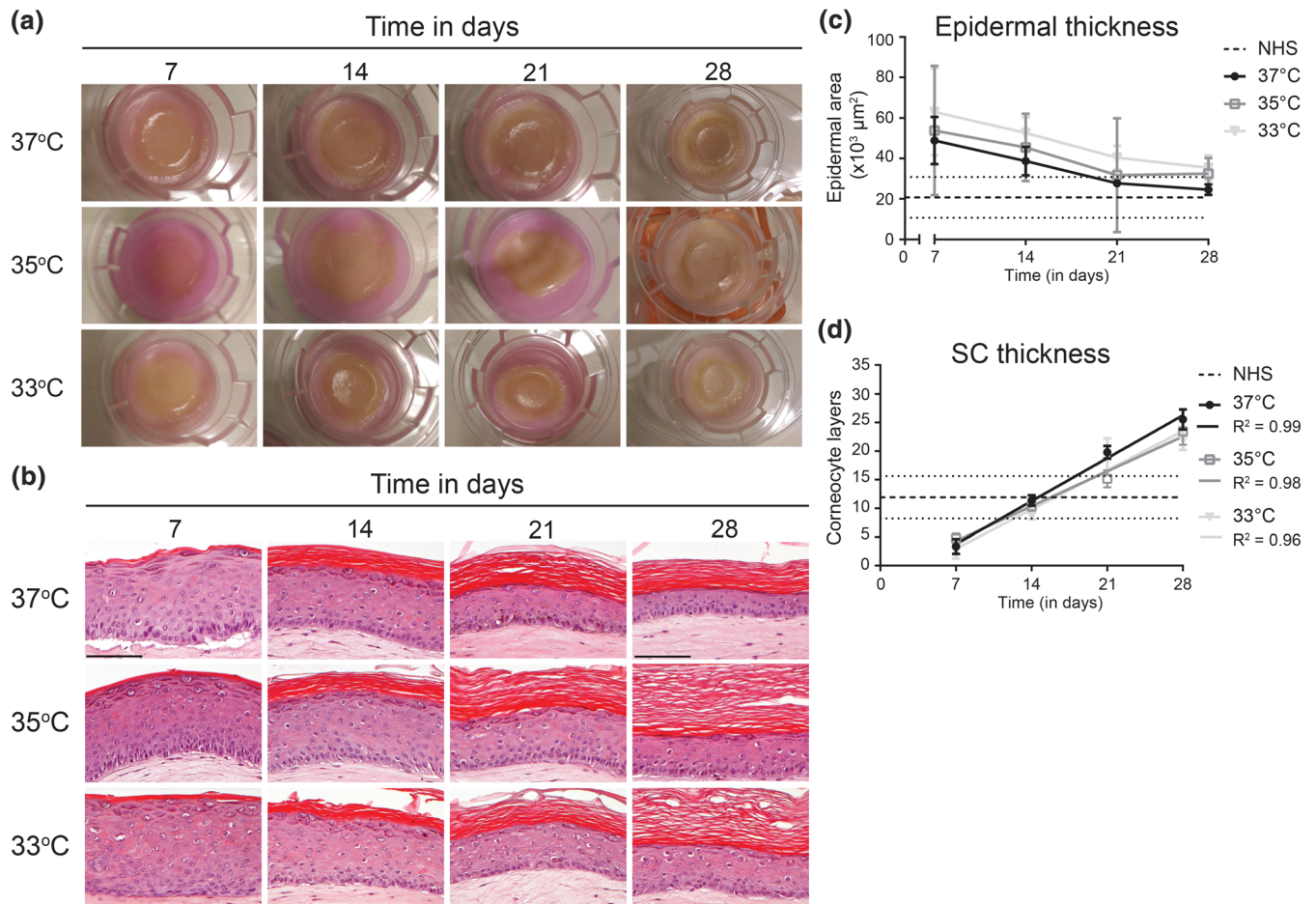
FIGURE 1 Generation of full thickness models (FTMs) at different temperatures over time. (a) Macroscopic images of FTMs in the culture system with support cotton pad. (b) Hematoxylin and eosin stained cross sections of FTMs developed over a 4-week time period. Scale bar indicates 100 μm. (c) Viable epidermal thickness in FTMs. Data presented with connection line and indicated range for NHS (not as function of time). (d) The number of corneocyte layers in the SC. Data fitted by a linear regression line. Range indication for NHS between dotted lines (not as function of time). Linear trend line formulas are $Y_{37°C} = 1,07X - 3,75$, $Y_{35°C} = 0,87X - 1,81$, and $Y_{33°C} = 0,98X - 3,89$. All data represent mean ± 95% confidence interval (CI), $n \geq 3$. NHS, native human skin; SC, stratum corneum [Colour figure can be viewed at wileyonlinelibrary.com]

FTMs generated at 33°C after 21 and 28 days in culture (Figure 3b). At FTMs developed at 35°C, there was no significant difference in the melanin content irrespective of time compared with 37°C.

3.4 | SC lipid matrix composition

Epidermal barrier formation was investigated by examination of the SC lipid matrix composition. The 12 most abundant CERs$_{total}$ subclasses of the intercorneocyte space were evaluated (Figure 4a). The CERs$_{total}$ from the lipid extract were detected as shown in the ion maps of FTMs generated at 14 days of culture (Figure S3), which were highly similar as those of FTMs 28 days air exposed (*data not shown*). Each CER subclass represents a series of CER entities due to the variation in chain length. In the ion maps of FTMs, we detected a high number of CER species with a mass below 600 amu, indicative for the presence of CERs with a short total carbon chain length. The ratio between lipids to extracted SC weight was unchanged after reducing the culture temperature and is comparable with that of NHS

(Figure 4b). To characterize the ceramide composition thoroughly, the CERs$_{total}$ composition was quantified into absolute amounts. The cumulative amounts of CERs$_{total}$ of FTMs and NHS were compared, which revealed a high similarity in total CER content (Figure 4c). Due to the presence of lower mass CERs on the ion maps of FTMs, we determined the average carbon chain length of CERs and CERs EO separately (Figure 4d,e). The average carbon chain length of CERs is similar in most FTMs but is significantly reduced compared with that in NHS. In FTMs generated at 33°C, the shortest average chain length was observed of CERs and CERs EO. Nonetheless, the average chain length of CERs EO resembled that of NHS to a high extent. When focusing on carbon chain length distribution, a higher level of C34–C42 CERs and a lower level of C42–C52 CERs were observed in FTMs compared with that in NHS, whereas in FTMs generated at 33°C, the C34–C42 CERs were higher and the C42–C52 CERs were lower than in FTMs generated at the two other temperatures (Figure S4a). In most conditions no differences were detected between FTMs and NHS regarding the CER EO chain length distribution, only in FTMs generated at the lowest temperature the distribution deviated
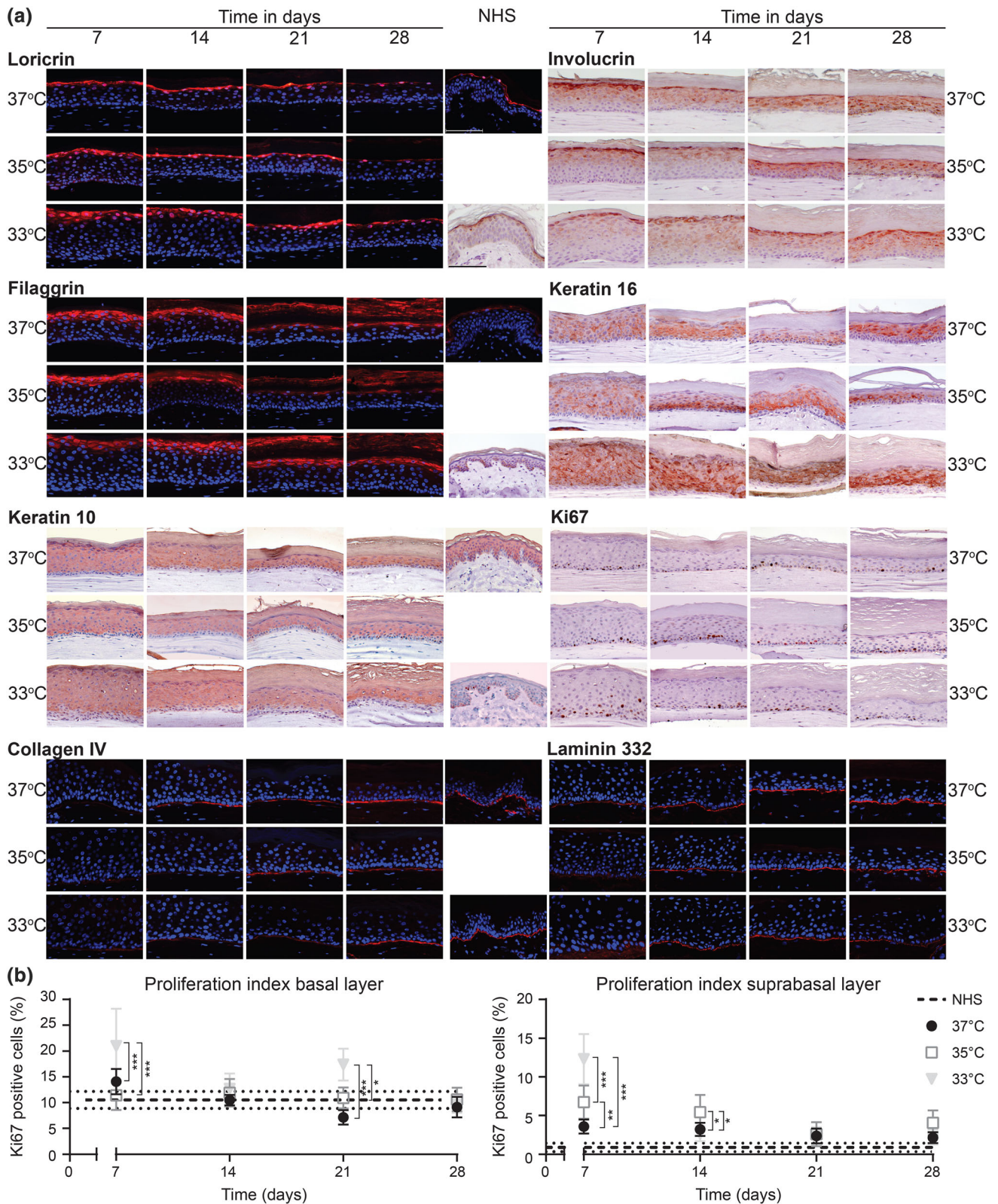
FIGURE 2 Epidermal morphogenesis in full thickness models generated at different temperatures over time. (a) Expression of protein biomarkers for the late and terminal differentiation programs (loricrin, involucrin, and filaggrin), epidermal activation (keratin 16), early differentiation (keratin 10), proliferation (Ki67), and basement membrane formation (collagen type IV and laminin 332). Protein expression is shown in full thickness models developed at different temperatures over time and in NHS (middle section). Nuclei are stained blue using haematoxylin or DAPI. Scale bar indicates 100 μm. (b) The number of Ki67 positive cells in the basal and suprabasal layer. The proliferation index of NHS is indicated by the horizontal dotted lines (not as function of time). Data represent mean ± 95% CI, $n \geq 3$. NHS, native human skin [Colour figure can be viewed at wileyonlinelibrary.com]
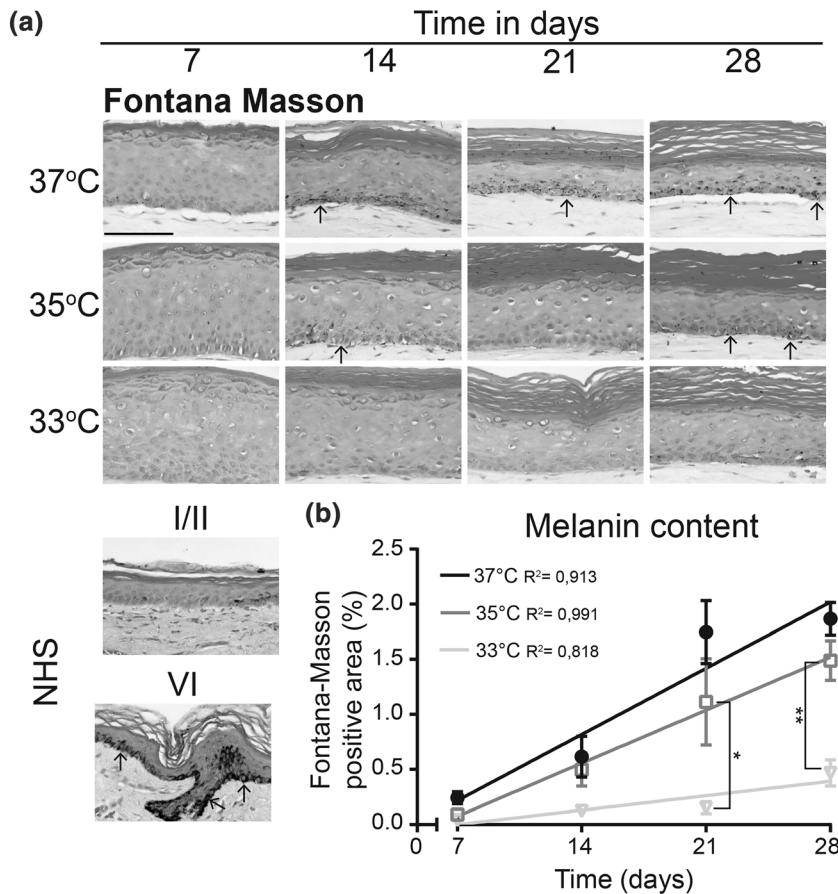
FIGURE 3 Melanogenesis in full thickness models generated at different temperatures over time. (a) Fontana-Masson silver staining of melanin in full thickness models developed at different temperatures over time and in NHS phenotype I/II and phenotype VI. Epidermis is counterstained with nuclear fast red. Arrowheads indicate melanin position. Scale bar indicates 100 μm. (b) Quantified melanin content in the viable epidermis plotted as Fontana-Masson positive area as percentage of the total area. Data represent mean ± *SEM*, $n \geq 2$, and are fitted with a linear regression line. NHS, native human skin

significantly from those generated at the other two temperatures (Figure S4b). Then, the CERs$_{total}$ subclass profiles of all FTMs and NHS were analysed, revealing a high similarity between the various culture temperatures in contrast to more substantial difference from that of NHS (Figure 4f,g). In FTMs generated at 33°C, the CERs$_{total}$ subclass profile deviated from FTMs generated at 37°C, as subclasses NS, AS, and EOS were significantly higher at 14 days culture deviating more from the subclass profile of NHS. Then, additional characteristics of CERs$_{total}$ were examined, starting with the level of unsaturated CERs. This is indicated by the percentage of monounsaturated as compared with the saturated CER, that is, the unsaturation index. Changes in the unsaturation index of CER AS and NS provide a good indication for differences in the level of unsaturated CERs$_{total}$ (unpublished data). In NHS, no unsaturated CERs were analysed due to their low abundance, but these are substantially present in FTMs. The unsaturation index is significantly higher in FTMs developed at 33°C after 14 days (Figure 4h). Over time, small changes in the unsaturation index were observed, albeit not significantly. Finally, the presence of glucosylceramides (GlcCERs) as an important CERs$_{total}$ precursor was determined. The level of GlcCERs is indicated by the ratio in area of GlcCER to its CER analogue, that is, the GlcCER index. This was determined for CERs EOS and EOH, as their GlcCER subclasses are processed exclusively by β-glucocerebrosidase. Furthermore, the CERs EO are very relevant for a proper SC lipid matrix structure. The GlcCERs were detected in the ion plots of FTMs and NHS (Figure S5a). Most GlcCERs were present in FTMs generated at the lowest

temperature, which were also elevated as compared with NHS (Figure S5b). When comparing the GlcCER indexes of FTMs over time, the GlcCERs index decreases after a longer culture period.

3.5 | Lipid organization

As a result of the composition, the lipids in the intercorneocyte space form a highly organized structure. To evaluate the effect of culture temperature on the lamellar organization, small-angle X-ray diffraction studies were performed. In the obtained diffraction peak profile, various orders of diffraction were identified (Figure 5a). The obtained diffraction patterns of the FTMs indicate only the presence of the long periodicity phase (LPP), whereas in NHS both the LPP and short periodicity phase have been detected (Bouwstra et al., 1991). No major differences were observed in the diffraction pattern of the FTMs developed at reduced temperatures, indicating similar phase behaviour. The peak position of the first, second, and third order of diffraction was used to calculate the repeat distance of the lipid lamellae in FTMs (Figure 5b). This revealed an equal repeat distance of the LPP in all tested conditions.

4 | DISCUSSION

The main objective of this study was to investigate the influence of culture temperature on epidermal morphogenesis and barrier
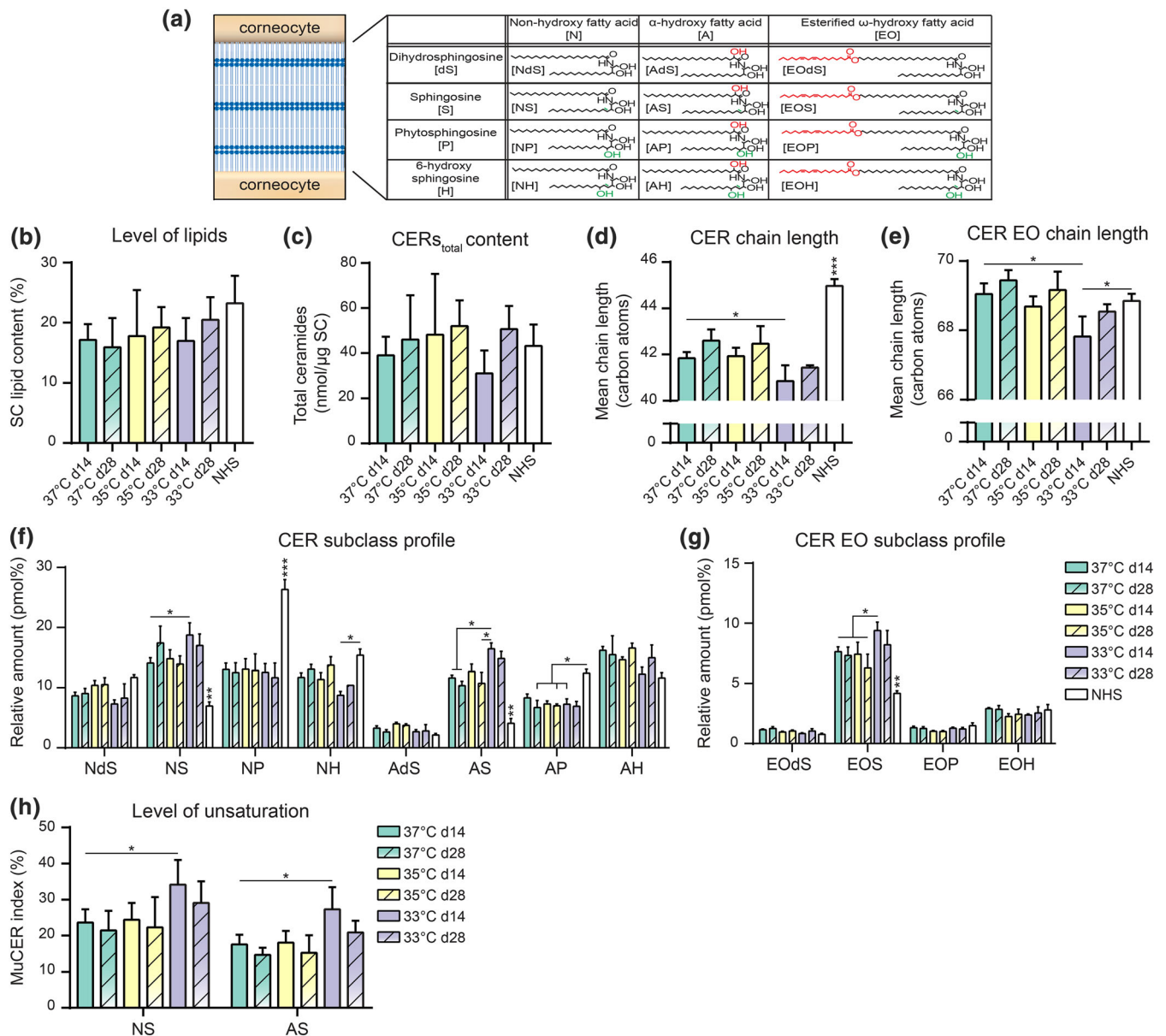
FIGURE 4 Barrier lipid composition in full thickness models (FTMs) generated at different temperatures over time. (a) Schematic overview of the intercorneocyte lipid matrix with a table of the 12 most abundant ceramide subclasses, modified from Janssens et al. (2012) with nomenclature of Motta et al. (1993). In the structure formulas, red parts indicate fatty acid based variations and green parts indicate sphingosine based variations. (b) Level of total lipids in the SC of indicated FTMs harvested at Day 14 (d14) and Day 28 (d28) after air exposure and of NHS. (c) Total amount of CERs per microgram SC in indicated FTMs and of NHS. (d) Bar diagram plot compares the average CERs carbon chain lengths of saturated CERs of indicated FTMs and NHS. (e) Bar diagram plot compares the average CERs EO carbon chain lengths of saturated CERs of indicated FTMs and NHS. (f) Saturated CER subclass profile of indicated FTMs and NHS. The total amount of saturated CERs has been set to 100%. (g) Saturated CER EO subclass profile of indicated FTMs and NHS. (h) Bar diagram plot compares the level of monounsaturation per ceramide subclass for CERs NS and AS of indicated FTMs. All data represent mean + SD, $n \geq 3$ (except in 33°C d28 where $n = 2$). Significance is shown for comparison between FTMs (with lines and asterisk) horizontally and for comparison of FTMs to NHS (vertically by NHS), otherwise indicated. Statistical differences are noted as *, **, or ***, corresponding to $p < .05$, $<.01$, and $<.001$. NHS, native human skin; SC, stratum corneum [Colour figure can be viewed at wileyonlinelibrary.com]

formation in HSEs. Our results demonstrate that reduction in culture temperature in FTMs augmented hyperplasia and leads to disorganization of the lower epidermal layers, indicated by the increased suprabasal proliferation and delayed early differentiation. In contrast, the late and terminal differentiation programs are weakly affected by culture temperature, and the corneocyte layers are formed at similar

rate. In line with terminal differentiation, the CERs$_{total}$ composition minimally differs at 35°C from that at 37°C but deviate in some aspects significantly at 33°C. Although in NHS, the skin surface temperature (28–32°C) is lower than the temperatures we tested in vitro (35°C and 33°C), closer approximation of in vivo temperatures used to generate FTMs is discouraged due to the higher
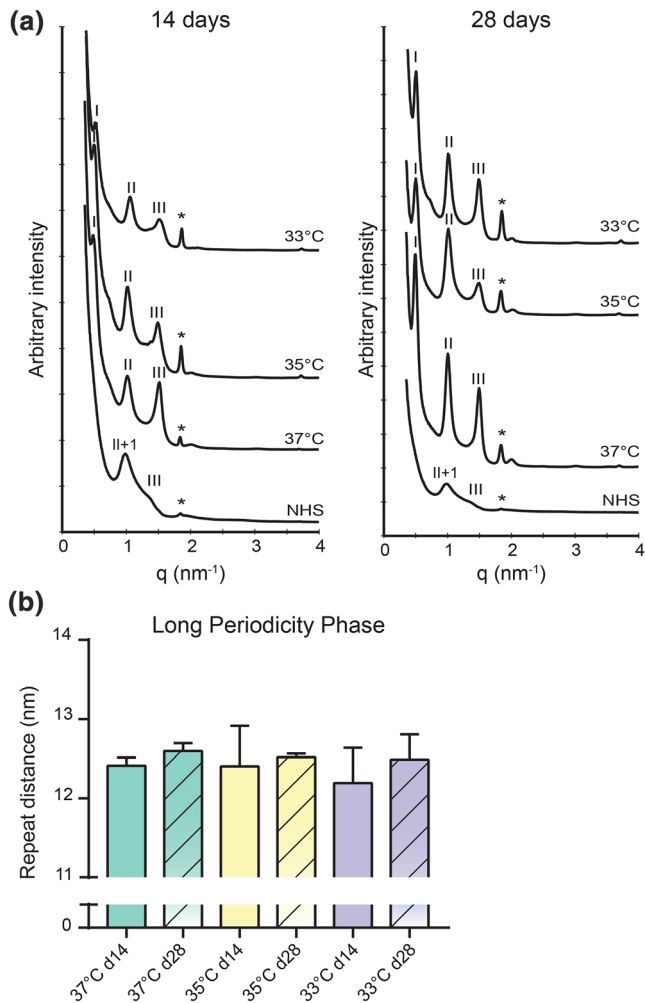
FIGURE 5 Lamellar organization within the lipid matrix. (a) Small angle X-ray diffraction patterns of full thickness models developed at different temperatures during 14 (d14) and 28 (d28) days air exposure combined with an identical NHS diffraction pattern. Long periodicity phase diffraction orders are indicated by roman numbers, short periodicity phase diffraction orders by Arabic numbers (NHS only), and the diffraction peak of phase separated cholesterol is indicated by the asterisk (*). (b) Bar diagram plot compares the repeat distance of the long periodicity phase. Data represent mean ± 95% CI, $n \geq 3$ (except in 33°C d28 where $n = 2$). NHS, native human skin [Colour figure can be viewed at wileyonlinelibrary.com]

disorganization of the lower epidermal layers at reduced culture temperature. This suggests that the lower epidermal layers are supported by temperatures closer to 37°C, indicating that the temperature gradient encountered in NHS plays an important role in the well-orchestrated epidermal morphogenesis.

Our findings are consistent with earlier results of keratinocytes grown on fibroblast-free de-epidermized dermis, at which the viable epidermis is thicker at 33°C compared with 37°C (Gibbs et al., 1997). Furthermore, our data are in agreement with previous findings from our group observed in HSEs and skin barrier repair explant model cultured at reduced temperature (32/33°C) regarding the delayed early differentiation (Danso et al., 2015; Ponec, Gibbs, et al., 1997). As in one of these models the basement membrane is already established, the dermal and basement membrane structure are unlikely to induce the observed disorganization in the lower region (Danso et al., 2015). Although our data differ to some extent from reports on the antiproliferating and pro-differentiating effect induced by lower culture temperature (Borowiec et al., 2013; Viano et al., 2017), it could be argued that the monolayer cultures of human keratinocytes, which demonstrated these effects on proliferation/differentiation, lack the epidermal calcium gradient and 3D epidermal structures, both important for epidermal homeostasis (Elias et al., 2002). Advantage of our approach is the use of 3D coculture models, which adds another aspect of complexity on how temperature reduction affects epidermal morphogenesis.

The main physical barrier of NHS and HSEs is formed by corneocytes, corneodesmosomes, tight junctions, and the lipid matrix (Basler et al., 2016; Haftek, 2015; Niehues et al., 2018). However, in this study, the lipid matrix was characterized, which is the only continuous pathway through the SC, and thereby regarded pivotal for the outside-in permeability barrier. The formation of the lipid barrier remains comparable at earlier and later time points, which is important for the performance of FTMs during long-term in vitro testing. At this detailed level, this has not been reported before. In our compositional analysis, the relative abundance of CERs EO is underestimated, because no unsaturated CERs EO with a linoleic acyl chain (contributing ~17–19% to FTM and NHS [unpublished data]) and saturated CERs EO with an oleic acyl chain (contributing ~23% to FTM [unpublished data]) were analysed. Nonetheless, the interpretation of the data is not affected by this. The increment in the level of CER subclasses AS and NS, which are observed in FTMs generated at 33°C are also observed in regenerated SC of ex vivo skin and in in vivo diseased skin conditions (Boiten et al., 2018; Danso et al., 2015; Van Smeden et al., 2014). Hence, these specific subclass alterations in several skin conditions could be linked to epidermal homeostatic imbalance, additionally emphasized by an upregulated keratin 16 expression. Furthermore, the ceramide composition contributes to the barrier functionality, as demonstrated in in vivo (diseased) skin conditions (Coderch, López, de la Maza, & Parra, 2003; Janssens et al., 2012), in HSEs (Mieremet, et al., 2017; Thakoersing et al., 2011), and in pure lipid model membranes (Groen, Poole, Gooris, & Bouwstra, 2011; Mojumdar, Helder, Gooris, & Bouwstra, 2014; Školová et al., 2013), suggesting a similar or reduced barrier functionality at lowered culture temperature. The CERs$_{total}$ precursors GlcCERs are less abundant at a later time point, possibly ascribed to more activity of β-glucocerebrosidase over time or to the maturation of the stratum granulosum - stratum corneum interface over time indicated by the flattening of the granular cells (Takagi, Kriehuber, Imokawa, Elias, & Holleran, 1999). The normalization in GlcCER content over time could also improve the barrier functionality, because impairment in the formation and conversion negatively affects the barrier functionality (Holleran et al., 1994; Jennemann et al., 2007; Sochorová et al., 2017).

In line with the result of the lipid composition, the lamellar organization is unaltered irrespective of the culture temperature and time. In the SC of FTMs, only LPP and no short periodicity phase was

observed, which is attributed especially to an increased level of CERs EO, but other factors may also play a role (Thakoersing et al., 2013). As compared with the reported 13.4 nm repeat distance of the LPP in NHS, the repeat distance of the LPP in FTMs is shortened (Bouwstra et al., 1991).

An interesting and not yet reported observation is the pigmentation in the epidermis of FTMs over time. In FTMs generated at reduced temperature, the pigmentation was reduced and/or delayed. Although melanocytes were not added to the FTM intentionally, during isolation of primary keratinocytes and subsequent culturing of these in keratinocyte culture medium, a small subset of melanocyte cells survived and induced pigmentation in FTMs. The Fontana-Masson silver positive staining in parts of the SC is most likely caused by non-specific staining silver deposition in the SC as suggested earlier (Joly-Tonetti, Wibawa, Bell, & Tobin, 2016). Our results are consistent with previous work by Kim et al. (2003), who suggested that temperature may affect the activity of key melanogenic enzyme tyrosinase. However, further research is required to gain more insights on the possible association between fibroblast-melanocyte crosstalk in HSEs (Wang et al., 2017), lower epidermal region disorganization, culture temperature, and pigmentation.

In conclusion, our results show that culture temperature strongly affects epidermal morphogenesis and melanogenesis but the barrier formation to a lesser extent. External conditions during in vitro tissue engineering play an important role and should be optimal to enhance the resemblance of HSEs to native skin tissue.

ACKNOWLEDGEMENTS

CONFLICT OF INTEREST

The authors declare no conflict of interest.

ORCID

Arnout Mieremet https://orcid.org/0000-0002-8330-7491

REFERENCES

Basler, K., Bergmann, S., Heisig, M., Naegel, A., Zorn-Kruppa, M., & Brandner, J. M. (2016). The role of tight junctions in skin barrier function and dermal absorption. *Journal of Controlled Release*, *242*, 105–118. https://doi.org/10.1016/j.jconrel.2016.08.007

Bidaux, G., Borowiec, A.-S., Gordienko, D., Beck, B., Shapovalov, G. G., Lemonnier, L., ... Prevarskaya, N. (2015). Epidermal TRPM8 channel isoform controls the balance between keratinocyte proliferation and differentiation in a cold-dependent manner. *Proceedings of the National Academy of Sciences*, *112*(26), E3345–E3354. https://doi.org/10.1073/pnas.1423357112

Bidaux, G., Borowiec, A.-S., Prevarskaya, N., & Gordienko, D. (2016). Fine-tuning of eTRPM8 expression and activity conditions keratinocyte fate. *Channels*, *10*(4), 320–331. https://doi.org/10.1080/19336950.2016.1168551

Boiten, W., Absalah, S., Vreeken, R., Bouwstra, J., & Van Smeden, J. (2016). Quantitative analysis of ceramides using a novel lipidomics approach with three dimensional response modelling. *Biochimica et Biophysica Acta (BBA)-Molecular and Cell Biology of Lipids*, *1861*(11), 1652–1661. https://doi.org/10.1016/j.bbalip.2016.07.004

Boiten, W. A., Berkers, T., Absalah, S., Van Smeden, J., Lavrijsen, A. P. M., & Bouwstra, J. A. (2018). Applying a vernix caseosa based formulation accelerates skin barrier repair by modulating lipid biosynthesis. *Journal of Lipid Research*, *59*(2), 250–260. https://doi.org/10.1194/jlr.M079186

Boncheva, M. (2014). The physical chemistry of the stratum corneum lipids. *International Journal of Cosmetic Science*, *36*(6), 505–515. https://doi.org/10.1111/ics.12162

Borowiec, A.-S., Delcourt, P., Dewailly, E., & Bidaux, G. (2013). Optimal differentiation of in vitro keratinocytes requires multifactorial external control. *PLoS ONE*, *8*(10), e77507. https://doi.org/10.1371/journal.pone.0077507

Bouwstra, J. A., Gooris, G. S., van der Spek, J. A., & Bras, W. (1991). Structural investigations of human stratum corneum by small-angle X-ray scattering. *Journal of Investigative Dermatology*, *97*(6), 1005–1012. https://doi.org/10.1111/1523-1747.ep12492217

Bouwstra, J. A., Honeywell-Nguyen, P. L., Gooris, G. S., & Ponec, M. (2003). Structure of the skin barrier and its modulation by vesicular formulations. *Progress in Lipid Research*, *42*(1), 1–36. https://doi.org/10.1016/S0163-7827(02)00028-0

Boyce, S. T. (1996). Cultured skin substitutes: A review. *Tissue Engineering*, *2*(4), 255–266. https://doi.org/10.1089/ten.1996.2.255

Coderch, L., López, O., de la Maza, A., & Parra, J. L. (2003). Ceramides and skin function. *American Journal of Clinical Dermatology*, *4*(2), 107–129. https://doi.org/10.2165/00128071-200304020-00004

Danso, M. O., Berkers, T., Mieremet, A., Hausil, F., & Bouwstra, J. A. (2015). An ex vivo human skin model for studying skin barrier repair. *Experimental Dermatology*, *24*(1), 48–54. https://doi.org/10.1111/exd.12579

Eichner, A., Sonnenberger, S., Dobner, B., Hauß, T., Schroeter, A., & Neubert, R. H. H. (2016). Localization of methyl-branched ceramide [EOS] species within the long-periodicity phase in stratum corneum lipid model membranes: A neutron diffraction study. *Biochimica et Biophysica Acta (BBA) - Biomembranes*, *1858*(11), 2911–2922. https://doi.org/10.1016/j.bbamem.2016.09.002

El Ghalbzouri, A., Commandeur, S., Rietveld, M. H., Mulder, A. A., & Willemze, R. (2009). Replacement of animal-derived collagen matrix by human fibroblast-derived dermal matrix for human skin equivalent products. *Biomaterials*, *30*(1), 71–78. https://doi.org/10.1016/j.biomaterials.2008.09.002

Elias, P. M., Ahn, S. K., Denda, M., Brown, B. E., Crumrine, D., Kimutai, L. K., ... Feingold, K. R. (2002). Modulations in epidermal calcium regulate the expression of differentiation-specific markers. *Journal of Investigative Dermatology*, *119*(5), 1128–1136. http://doi.org/10.1046/j.1523-1747.2002.19512.x

Feingold, K. R., & Elias, P. M. (2014). Role of lipids in the formation and maintenance of the cutaneous permeability barrier. *Biochimica et Biophysica Acta (BBA) - Molecular and Cell Biology of Lipids*, *1841*(3), 280–294. https://doi.org/10.1016/j.bbalip.2013.11.007

Gibbs, S., Vicanová, J., Bouwstra, J., Valstar, D., Kempenaar, J., & Ponec, M. (1997). Culture of reconstructed epidermis in a defined medium at 33 degrees C shows a delayed epidermal maturation, prolonged lifespan

and improved stratum corneum. *Archives of Dermatological Research*, *289*(10), 585–595. https://doi.org/10.1007/s004030050244

Gordon, S., Daneshian, M., Bouwstra, J., Caloni, F., Constant, S., Davies, D. E., … Lehr, C. M. (2015). Non-animal models of epithelial barriers (skin, intestine and lung) in research, industrial applications and regulatory toxicology. *Alternatives to Animal Experimentation: ALTEX*, *32*(4), 327–378. https://doi.org/10.14573/altex.1510051

Groen, D., Poole, D. S., Gooris, G. S., & Bouwstra, J. A. (2011). Investigating the barrier function of skin lipid models with varying compositions. *European Journal of Pharmaceutics and Biopharmaceutics*, *79*(2), 334–342. https://doi.org/10.1016/j.ejpb.2011.05.007

Haftek, M. (2015). Epidermal barrier disorders and corneodesmosome defects. *Cell and Tissue Research*, *360*(3), 483–490. https://doi.org/10.1007/s00441-014-2019-1

Haisma, E. M., Rietveld, M. H., de Breij, A., van Dissel, J. T., El Ghalbzouri, A., & Nibbering, P. H. (2013). Inflammatory and antimicrobial responses to methicillin-resistant Staphylococcus aureus in an in vitro wound infection model. *PLoS ONE*, *8*(12), e82800. https://doi.org/10.1371/journal.pone.0082800

Holleran, W. M., Ginns, E. I., Menon, G. K., Grundmann, J. U., Fartasch, M., McKinney, C. E., … Sidransky, E. (1994). Consequences of beta-glucocerebrosidase deficiency in epidermis. Ultrastructure and permeability barrier alterations in Gaucher disease. *Journal of Clinical Investigation*, *93*(4), 1756–1764. https://doi.org/10.1172/JCI117160

Janssens, M., van Smeden, J., Gooris, G. S., Bras, W., Portale, G., Caspers, P. J., … Bouwstra, J. A. (2012). Increase in short-chain ceramides correlates with an altered lipid organization and decreased barrier function in atopic eczema patients. *Journal of Lipid Research*, *53*(12), 2755–2766. https://doi.org/10.1194/jlr. P030338

Jennemann, R., Sandhoff, R., Langbein, L., Kaden, S., Rothermel, U., Gallala, H., … Gröne, H. J. (2007). Integrity and barrier function of the epidermis critically depend on glucosylceramide synthesis. *Journal of Biological Chemistry*, *282*(5), 3083–3094. https://doi.org/10.1074/jbc.M610304200

Joly-Tonetti, N., Wibawa, J. I. D., Bell, M., & Tobin, D. (2016). Melanin fate in the human epidermis: A reassessment of how best to detect and analyse histologically. *Experimental Dermatology*, *25*(7), 501–504. https://doi.org/10.1111/exd.13016

Kim, D.-S., Park, S.-H., Kwon, S.-B., Joo, Y. H., Youn, S. W., Sohn, U. D., & Park, K. C. (2003). Temperature regulates melanin synthesis in melanocytes. *Archives of Pharmacal Research*, *26*(10), 840–845. https://doi.org/10.1007/BF02980030

Mieremet, A., Rietveld, M., Absalah, S., Van Smeden, J., Bouwstra, J. A., & El Ghalbzouri, A. (2017). Improved epidermal barrier formation in human skin models by chitosan modulated dermal matrices. *PLoS ONE*, *12*(3), e0174478. https://doi.org/10.1371/journal.pone.0174478

Mieremet, A., Rietveld, M., van Dijk, R., Bouwstra, J. A., & El Ghalbzouri, A. (2018). Recapitulation of native dermal tissue in a full-thickness human skin model using human collagens. *Tissue Engineering Part A*, *24*(11), 873–881. https://doi.org/10.1089/ten.tea.2017.0326

Mojumdar, E., Kariman, Z., van Kerckhove, L., Gooris, G. S., & Bouwstra, J. A. (2014). The role of ceramide chain length distribution on the barrier properties of the skin lipid membranes. *Biochimica et Biophysica Acta (BBA) - Biomembranes*, *1838*(10), 2473–2483. https://doi.org/10.1016/j.bbamem.2014.05.023

Mojumdar, E. H., Gooris, G. S., Groen, D., Barlow, D. J., Lawrence, M. J., Demé, B., & Bouwstra, J. A. (2016). Stratum corneum lipid matrix: Location of acyl ceramide and cholesterol in the unit cell of the long periodicity phase. *Biochimica et Biophysica Acta (BBA) - Biomembranes*, *1858*(8), 1926–1934. https://doi.org/10.1016/j.bbamem.2016.05.006

Mojumdar, E. H., Helder, R. W., Gooris, G. S., & Bouwstra, J. A. (2014). Monounsaturated fatty acids reduce the barrier of stratum corneum lipid membranes by enhancing the formation of a hexagonal lateral packing. *Langmuir*, *30*(22), 6534–6543. https://doi.org/10.1021/la500972w

Motta, S., Monti, M., Sesana, S., Caputo, R., Carelli, S., & Ghidoni, R. (1993). Ceramide composition of the psoriatic scale. *Biochimica et Biophysica Acta (BBA) - Molecular Basis of Disease*, *1182*(2), 147–151. https://doi.org/10.1016/0925-4439(93)90135-N

Niehues, H., Bouwstra, J. A., El Ghalbzouri, A., Brandner, J. M., Zeeuwen, P. L., & van den Bogaard, E. H. (2018). 3D skin models for 3R research: The potential of 3D reconstructed skin models to study skin barrier function. *Experimental Dermatology*, *27*(5), 501–511. https://doi.org/10.1111/exd.13531

Pinnagoda, J., Tupkek, R., Agner, T., & Serup, J. (1990). Guidelines for transepidermal water loss (TEWL) measurement. *Contact Dermatitis*, *22*(3), 164–178. https://doi.org/10.1111/j.1600-0536.1990.tb01553.x

Planz, V., Lehr, C.-M., & Windbergs, M. (2016). In vitro models for evaluating safety and efficacy of novel technologies for skin drug delivery. *Journal of Controlled Release*, *242*, 89–104. https://doi.org/10.1016/j.jconrel.2016.09.002

Ponec, M., Gibbs, S., Weerheim, A., Kempenaar, J., Mulder, A., & Mommaas, A. M. (1997). Epidermal growth factor and temperature regulate keratinocyte differentiation. *Archives of Dermatological Research*, *289*(6), 317–326. https://doi.org/10.1007/s004030050198

Ponec, M., Weerheim, A., Kempenaar, J., Mommaas, A. M., & Nugteren, D. H. (1988). Lipid composition of cultured human keratinocytes in relation to their differentiation. *Journal of Lipid Research*, *29*(7), 949–961.

Ponec, M., Weerheim, A., Kempenaar, J., Mulder, A., Gooris, G. S., Bouwstra, J., & Mieke Mommaas, A. (1997). The formation of competent barrier lipids in reconstructed human epidermis requires the presence of vitamin C. *Journal of Investigative Dermatology*, *109*(3), 348–355. https://doi.org/10.1111/1523-1747.ep12336024

Proksch, E., Brandner, J. M., & Jensen, J.-M. (2008). The skin: An indispensable barrier. *Experimental Dermatology*, *17*(12), 1063–1072. https://doi.org/10.1111/j.1600-0625.2008.00786.x

Regnier, M., Caron, D., Reichert, U., & Schaefer, H. (1993). Barrier function of human skin and human reconstructed epidermis. *Journal of Pharmaceutical Sciences*, *82*(4), 404–407. https://doi.org/10.1002/jps.2600820414

Schmook, F. P., Meingassner, J. G., & Billich, A. (2001). Comparison of human skin or epidermis models with human and animal skin in in-vitro percutaneous absorption. *International Journal of Pharmaceutics*, *215*(1), 51–56. https://doi.org/10.1016/S0378-5173(00)00665-7

Schreiber, S., Mahmoud, A., Vuia, A., Rübbelke, M. K., Schmidt, E., Schaller, M., … Schäfer-Korting, M. (2005). Reconstructed epidermis versus human and animal skin in skin absorption studies. *Toxicology In Vitro*, *19*(6), 813–822. https://doi.org/10.1016/j.tiv.2005.04.004

Školová, B., Janůšová, B., Zbytovská, J., Gooris, G., Bouwstra, J., Slepička, P., … Vávrová, K. (2013). Ceramides in the skin lipid membranes: Length matters. *Langmuir*, *29*(50), 15624–15633. https://doi.org/10.1021/la4037474

Sochorová, M., Staňková, K., Pullmannová, P., Kováčik, A., Zbytovská, J., & Vávrová, K. (2017). Permeability barrier and microstructure of skin lipid membrane models of impaired glucosylceramide processing. *Scientific Reports*, *7*(6470), 1–8. https://doi.org/10.1038/s41598-017-06990-7

Stark, H.-J., Baur, M., Breitkreutz, D., Mirancea, N., & Fusenig, N. E. (1999). Organotypic keratinocyte cocultures in defined medium with regular epidermal morphogenesis and differentiation. *Journal of Investigative Dermatology*, *112*(5), 681–691. https://doi.org/10.1046/j.1523-1747.1999.00573.x

Takagi, Y., Kriehuber, E., Imokawa, G., Elias, P. M., & Holleran, W. M. (1999). β-Glucocerebrosidase activity in mammalian stratum corneum. *Journal of Lipid Research*, 40(5), 861–869.

Thakoersing, V. S., Gooris, G. S., Mulder, A., Rietveld, M., El Ghalbzouri, A., & Bouwstra, J. A. (2011). Unraveling barrier properties of three different in-house human skin equivalents. *Tissue Engineering Part C: Methods*, 18(1), 1–11. https://doi.org/10.1089/ten.tec.2011.0175

Thakoersing, V. S., van Smeden, J., Mulder, A. A., Vreeken, R. J., El Ghalbzouri, A., & Bouwstra, J. A. (2013). Increased presence of mono-unsaturated fatty acids in the stratum corneum of human skin equivalents. *Journal of Investigative Dermatology*, 133(1), 59–67. https://doi.org/10.1038/jid.2012.262

van Drongelen, V., Danso, M. O., Mulder, A., Mieremet, A., Van Smeden, J., Bouwstra, J. A., & El Ghalbzouri, A. (2014). Barrier properties of an N/TERT-based human skin equivalent. *Tissue Engineering Part A*, 20(21–22), 3041–3049. https://doi.org/10.1089/ten.tea.2014.0011

Van Smeden, J., Janssens, M., Boiten, W. A., Van Drongelen, V., Furio, L., Vreeken, R. J., ... Bouwstra, J. A. (2014). Intercellular skin barrier lipid composition and organization in Netherton syndrome patients. *Journal of Investigative Dermatology*, 134(5), 1238–1245. https://doi.org/10.1038/jid.2013.517

Viano, M., Alotto, D., Aillon, A., Castagnoli, C., & Silvagno, F. (2017). A thermal gradient modulates the oxidative metabolism and growth of human keratinocytes. *FEBS Open Bio*, 7, 1843–1853. https://doi.org/10.1002/2211-5463.12303

Wang, Y., Viennet, C., Robin, S., Berthon, J. Y., He, L., & Humbert, P. (2017). Precise role of dermal fibroblasts on melanocyte pigmentation. *Journal of Dermatological Science*, 88(2), 159–166. https://doi.org/10.1016/j.jdermsci.2017.06.018

SUPPORTING INFORMATION

Additional supporting information may be found online in the Supporting Information section at the end of the article.

Table S1 Specification of antibodies used for immunohistochemical and immunofluorescence staining.

Figure S1. Negative controls of immunohistochemistry and safranin red staining of stratum corneum. (a) Experimental negative controls of immunohistochemistry and immunofluorescence stainings. Nuclei are stained blue using haematoxylin or DAPI. **(b)** Representative cross sections of FTMs and NHS stained with safranin red followed by alkali induced expansion of the stratum corneum used for quantification of the amount of corneocyte layers. Scale bar indicates 100 μm.

Figure S2. Three dimensional response model for quantification of CERs$_{total}$. This 3D response model is used for quantification of the CERs$_{total}$ composition. Model is based on i) mass spectrometry settings, ii) compound properties and a calibration curve from a limited number of synthetic ceramides, as described by Boiten et al. (Boiten, Absalah, Vreeken, Bouwstra, & van Smeden, 2016).

Figure S3. Ion maps of FTMs developed at different temperatures after 14 days air-exposed and of NHS. Positions and names of ceramide subclasses are indicated in the ion map of NHS.

Figure S4. Ceramide carbon chain length distribution of FTMs and NHS. (a) Bar diagram plot of CERs with an even number of carbon atoms of FTMs generated at different temperatures during 14 and 28 days air-exposure and of NHS. **(b)** Bar diagram plot of even numbered CERs EO of FTMs generated at different temperatures during 14 and 28 days air-exposure and of NHS. The saturated CERs$_{total}$ has been set to 100%. Data represent mean + SEM, $n \geq 3$ (except 33°C d28 where $n = 2$). Significance is shown for comparison between FTMs (with lines and asterisk) horizontally and for comparison of FTMs to NHS (vertically by NHS), otherwise indicated. Statistical differences are noted as *, ** or ***, corresponding to $P < 0.05$, <0.01, <0.001.

Figure S5. Glucosylceramides in the lipid matrix of FTMs and NHS. (a) Ion plots of glucosylceramides as detected by LC–MS in FTMs developed for 14 days at 3 different temperatures and of NHS. Position and name of glucosyl-EOS and -EOH (Glc-EOS and Glc-EOH) are indicated in the ion plot of NHS. **(b)** Bar diagram plot compares the glucosylceramide index of indicated FTMs and NHS based on the ratio of CERs EOS and EOH to their glucosylated analogues Glc-EOS and Glc-EOH, as described earlier (van Smeden, et al., 2017). Data represent mean + SD, $n \geq 3$ (except 33°C d28 where $n = 2$).